NUMERICAL SIMULATION OF HIGH-INCIDENCE FLOW OVER THE F-18 AIRCRAFT

Russell M. Cummings*, Lewis B. Schiff**, Yehia M. Rizk†, and Neal M. Chaderjian†
NASA Ames Research Center, Moffett Field, CA, USA

Abstract

Navier-Stokes solutions have been obtained using the Chimera overset grid scheme for flow over the wing, fuselage, and wing leading-edge extension (LEX) of the F-18 aircraft at high incidence. Solutions are also presented for flow over the fuselage forebody at high angles of attack. The solutions are for turbulent flows at high-Reynolds-number flight-test conditions, and are compared with available qualitative and quantitative experimental data. Comparisons of predicted surface flow patterns, off-surface flow visualizations, and surface-pressure distributions are in good agreement with flight-test data. The ability of the numerical method to predict the bursting of the LEX vortex as it encounters the adverse pressure gradient field of the wing is demonstrated.

Introduction

A high angle-of-attack technology program is currently underway within NASA. The objectives of the program include the development of flight-validated design methods which accurately predict the aerodynamics and flight dynamics of aircraft maneuvering in the high-angle-of-attack regime. Toward meeting these objectives, the program integrates ground-based experimental and computational investigations, currently underway at the NASA Ames, Langley, and Lewis Research Centers, with flight-test investigations being conducted on the F/A-18 High Alpha Research Vehicle (HARV) at the Ames-Dryden Flight Research Facility. These tests include surface and off-surface flow visualizations, as well as quantitative measurements of the flow surrounding the HARV at large incidence. This paper presents results of Navier-Stokes computations of the flow about the wing, fuselage, and wing leading-edge extension of the F-18 HARV at conditions matching those of the flight tests. Previous numerical predictions for the isolated F-18 fuselage forebody were reported in Refs. 1 - 3.

Numerical prediction of the flow over aircraft flying at large angles of attack is a difficult aerodynamic problem. High-angle-of-attack flows contain large regions of three-dimensional separated flow, where the boundary layers leave the surface of the body along surfaces of separation, and roll up on the leeward side of the body to form strong, concentrated vortical flows. Separated flows have historically been treated by a wide variety of computational methods, ranging from simple potential flow methods to time-marching Navier-Stokes techniques. However, the close coupling which exists between the strength and location of the leeward vortical flow and the location of the viscous layer separation lines has precluded accurate predictions of high-incidence flow with the more approximate techniques.

The recent introduction of supercomputers such as the CRAY 2 and CRAY YMP has permitted a quantum increase in the size of computational grids. As a result, it is now possible to compute high-angle-of-attack flows over bodies and aircraft components with codes based on the Reynolds-averaged Navier-Stokes equations, and use sufficient grid points to adequately resolve the main features of the three-dimensional separated flow field (cf. Refs. 4 - 10). In conjunction with this increase in computer capability, effective numerical tools are being developed which properly model the fundamental fluid dynamic processes which occur at high angles of attack. Consequently, we have focused solely on time-marching Navier-Stokes computations, and have used the three-dimensional partially flux-split, Navier-Stokes code reported by Steger et al.[11] Several of the more important numerical and physical concerns which must be addressed for accurate numerical predictions of high-incidence flows have been identified and discussed in a previous work.[12] Also, in order to model complex geometries, the Chimera overset grid approach[13,14] has been utilized. The Chimera scheme allows for combining grids about individual body components (such as the fuselage or wing) and obtaining a flowfield solution without the need for matching grid points at zonal interfaces. The end result will be a set of numerical tools which will enable researchers to confidently predict flow over aircraft at high angles of attack.

Theoretical Background

Governing Equations

The conservation equations of mass, momentum, and energy can be represented in a flux-vector form that is convenient for numerical solution as[15]

$$\partial_\tau \hat{Q} + \partial_\xi(\hat{F} + \hat{F}_v) + \partial_\eta(\hat{G} + \hat{G}_v) + \partial_\zeta(\hat{H} + \hat{H}_v) = 0 \quad (1)$$

where τ is the time, and the independent spatial variables, ξ, η, and ζ are chosen to map a curvilinear body-conforming grid into a uniform computational space (see

---

* National Research Council Research Associate. Associate Professor, on leave from California Polytechnic State University, Aeronautical Engineering Department.

** Special Assistant for High Alpha Technology, Fluid Dynamics Division.

†Research Scientist, Applied Computational Fluids Branch.

Fig. 1). In Eq. (1) $\hat{Q}$ is the vector of dependent flow variables; $\hat{F} = \hat{F}(\hat{Q})$, $\hat{G} = \hat{G}(\hat{Q})$, and $\hat{H} = \hat{H}(\hat{Q})$ are the inviscid flux vectors, while the terms $\hat{F}_v$, $\hat{G}_v$, and $\hat{H}_v$ are fluxes containing the viscous derivatives. A nondimensional form of the equations is used throughout this work. Density is normalized by the free-stream density, ρ_∞, the velocity components are normalized by the free-stream speed of sound, a_∞, and pressure is normalized by $\rho_\infty a_\infty^2$.

For body-conforming coordinates and high-Reynolds number flow, if ζ is the coordinate leading away from the surface, the thin-layer approximation can be applied, which yields[16,17]

$$\partial_\tau \hat{Q} + \partial_\xi \hat{F} + \partial_\eta \hat{G} + \partial_\zeta \hat{H} = Re^{-1} \partial_\zeta \hat{S} \tag{2}$$

where only viscous terms in the ζ direction are retained. These have been collected into the vector $\hat{S}$ and the Reynolds number, Re, is factored from the viscous flux term. A more detailed development and explanation of the form of the governing equations which have been solved can be found in Ref. 11.

Turbulence Model

The coefficients of viscosity and thermal conductivity which appear in Eq. (2) are specified from auxiliary relations. For laminar flow the coefficient of viscosity is obtained using Sutherland's law. For turbulent flow the coefficient is obtained from the eddy-viscosity turbulence model reported by Baldwin and Lomax[16] for the wing, and from the modified Baldwin-Lomax model reported by Degani and Schiff[18] for the fuselage. The coefficient of thermal conductivity is obtained, once the viscosity coefficient is known, by assuming a constant Prandtl number.

Degani and Schiff developed a modification to the well-known Baldwin-Lomax[16] model (which is itself based on the two-layer model reported by Cebeci, Smith, and Mosinkis[19]). As proposed by Baldwin and Lomax, the turbulence model examines a quantity containing the local fluid vorticity magnitude to determine the length scale, and thus the eddy viscosity coefficient. The modifications made by Degani and Schiff[18] permit the model to differentiate between the vorticity within the attached boundary layers and the vorticity on the surfaces of separation, and therefore to select a length scale based on the thickness of the attached boundary layers rather than one based on the normal distance between the body surface and the surface of separation. Thus, the modifications extend the model in a rational manner to permit an accurate determination of the viscous length scale for high-angle-of-attack flows in regions of crossflow separation, where a strong leeward vortical flow structure exists.

Numerical Algorithm

The implicit scheme employed in this study is the F3D algorithm reported by Steger et al. in Ref. 11. The algorithm uses flux-vector splitting[20] to upwind difference the convection terms in one coordinate direction (nominally streamwise). As discussed in Ref. 11, schemes using upwind differencing can have several advantages over methods which utilize central spatial differences in each direction. In particular, such schemes can have natural numerical dissipation and better stability properties. By using upwind differencing for the convective terms in the streamwise direction while retaining central differencing in the other directions, a two-factor implicit approximately-factored algorithm is obtained, which has been shown to be unconditionally stable[21] for a representative model wave equation. The scheme may be written for the thin-layer Navier-Stokes equations in the form

$$\begin{aligned}
&\Big[I + i_b\Big(h\delta_\xi^b(\hat{A}^+)^n + h\delta_\zeta \hat{C}^n - hRe^{-1}\bar{\delta}_\zeta J^{-1}\hat{M}^n J - D_i|_\zeta\Big)\Big] \\
&\quad \times \Big[I + i_b\Big(h\delta_\xi^f(\hat{A}^-)^n + h\delta_\eta \hat{B}^n - D_i|_\eta\Big)\Big]\Delta\hat{Q}^n = \\
&\quad - i_b\Delta t\{\delta_\xi^b(\hat{F}^+)^n + \delta_\xi^f(\hat{F}^-)^n + \delta_\eta(\hat{G}^n) + \delta_\zeta(\hat{H}^n) \\
&\quad - Re^{-1}\bar{\delta}_\zeta(\hat{S}^n)\} - i_b D_e(\hat{Q}^n)
\end{aligned} \tag{3}$$

where $h = \Delta t$ or $\Delta t/2$ for first- or second-order time accuracy, and the free-stream base solution is used, denoted by the subscript ∞. Second-order time accuracy is used when a nonsteady solution is required. In Eq. (3) δ is typically a three-point, second-order-accurate, central difference operator, $\bar{\delta}$ is a midpoint operator used with the viscous terms, and the operators δ_ξ^b and δ_ξ^f are backward and forward three-point difference operators. The flux $\hat{F}$ has been split into $\hat{F}^+$ and $\hat{F}^-$, according to the sign of the eigenvalues of the Jacobian matrix,[20] and the matrices, $\hat{A}^\pm, \hat{B}, \hat{C}$, and $\hat{M}$ result from local linearization of the fluxes about $\hat{F}$, $\hat{G}$, $\hat{H}$, and $\hat{S}$, respectively. J denotes the Jacobian of the coordinate transformation. Dissipation operators, D_e and D_i, are used in the central space-differencing directions. Full details of the development of the algorithm may be found in Refs. 11 and 21.

In applying the Chimera approach,[13,14,22] separate body-conforming grids are established individually around various components of the aircraft. Thus, the possibility exists of having arbitrary holes in a grid, for example, at grid points of the fuselage grid which lie within the wing. Similarly, the wing grid may have hole points due to the presence of the fuselage or another component. In the Chimera approach, each of the grids is advanced one step in time sequentially. When advancing the solution, the difference equations are turned off at such hole points to leave the solution unchanged. In order to turn off the differencing scheme at hole points, an array of values i_b is included in Eq. 3 such that $i_b = 1$ at normal grid points and $i_b = 0$ at hole points.

Each hole includes fringe points which are later updated by interpolation from the solution computed in the grid surrounding the component which created the hole. If only three-point central spatial differencing is used, the algorithm would require no other modifications. However, spatial operators that require information from points beyond those immediately adjacent to the differenced point would use information beyond the single-point hole fringe. Since only the fringe points are updated by interpolation from other grids, interior hole points do not contain meaningful data. Consequently, it is necessary to limit the

spatial difference operators adjacent to holes so that only the single adjacent fringe point is used. Specifically, the second-order accurate upwind difference operators and the explicit dissipation operators both contain five-point central fourth-order differencing, and must be modified. Also, in order to improve the accuracy of the solutions, the dissipation in the boundary layer is reduced in the fashion of Kaynak, Holst, and Cantwell.[23] In this region, large numerical smoothing terms can adversely affect the accuracy of the solution by modifying the physical viscous terms. Additional information about the precise formulation of the differencing operators and numerical dissipation may be found in Refs. 13, 14, and 22.

Geometry Modeling and Grid Generation

Even with the large memory size available on the CRAY 2 computer, it is not practical to develop a single-block grid which includes the geometric complexity of a complete aircraft. Thus, for computations of the complete HARV configuration, a multi-block grid will be needed (cf. Refs. 24 and 25 for examples of multi-block Navier-Stokes computations of flow over a complete aircraft configuration in transonic, low-incidence flow). In the present computations of flow over the F-18, the decision to use a multi-block grid was strongly influenced by the complexities of the geometry, including the LEX, wing/LEX junction, and inlet. For this study, results will be shown for computations over the fuselage forebody as well as for the wing/fuselage geometry.

Geometry Modeling

The correct representation of the aircraft surface geometry is required prior to creating the computational grids, and thus has an essential role in accurate numerical simulation of the flowfield. Since the surface geometry of the F-18 is quite complex, certain geometric simplifications have been adopted in this work. Those simplifications that have a significant effect on the computed flow will be relaxed in future studies. The simplifications include the omission of the inlet compression ramp and boundary layer diverter, and the fairing over of the engine inlet. This will lead to aerodynamic results similar to those for the aircraft flying at minimum power. The LEX slots have also been faired over. Finally, the fuselage geometry does not include various small "disruptions," such as antennae, hinges, rivets, etc.

The fuselage was extended aft of the wing by repeating the body cross-section found near the wing trailing edge. This cross-section maintains the definition of the LEX downstream of the wing, so a finite thickness flow-through cut was applied on the LEX surface aft of the wing in order to insure proper modeling. The body extends approximately eleven wing-root-chord lengths aft of the wing trailing edge.

The wing was modeled after a simplified representation of the F-18 wing geometry. The inboard chord sections of the wing are defined by a 5% thick NACA 65A airfoil, with a transition to a 3.5% thick section at approximately two-thirds span. The wing has 3° of negative dihedral and 4° of twist (wash-out near the tip chord), with 20° of sweepback along the quarter-chord. Although it is recognized that the wing leading-edge flap of the F-18 deflects downward as the angle of attack increases, the flap was modeled undeflected. Similarly, no attempt was made to model the missile launch rail or the deflection of other wing control surfaces. Both the wing and fuselage surface grids were slightly modified at the wing/fuselage junction in order to insure geometric matching at that location.

The simplified computational surface geometry for the F-18 is shown in Fig. 2. The fuselage surface grid was created using spline representations, with clustering in both the axial and circumferential directions. Control points were defined at surface junctions and edges, with spacing matched on both sides of the control points. The surface geometry and surface grid for the wing was generated using the S3D code,[26] with grid redistribution in both the spanwise and chordwise directions. The redistribution was done to cluster grid points near the wing tip and leading edge, and to relax them near the root and trailing edge. The wing-tip was closed (the actual wing geometry has a finite thickness at the wing tip) to a sharp tip, with the transition occurring over the five most outboard wing cross-sections (3% of the semi-span).

Grid Generation

Results will be shown for both isolated fuselage forebody and wing/fuselage numerical predictions. Two isolated forebody grids were employed; a single-block grid generated using a hyperbolic grid generation method,[27] and a two-block grid generated using an elliptic grid generation technique.[28] Further details of the isolated forebody grids can be found in Ref. 1.

The Chimera overset grid scheme[13,14,22] was used to allow treatment of the wing/fuselage configuration of the F-18 (see Fig. 3). This composite-grid approach allows the extension of a flow code valid for a single, ordered grid to be used to obtain solutions about complex configurations which require multiple grids. The Chimera approach permits minor grids to be generated separately about individual components of the configuration (such as the wing), and be overset onto a main grid which encompasses the entire configuration. The minor grids are used to resolve features of the geometry or flow that are not adequately resolved by the major grid.

The F-18 fuselage grid utilizes a C-O topology with 83 axial, 63 circumferential, and 49 radial points. The grid extends away from the fuselage surface approximately three wing-root-chord lengths. The grid was obtained using the same hyperbolic generation technique[27] as was used for the one-block fuselage forebody grid. Furthermore, a coarse far-field grid encloses the fuselage grid and extends over twenty wing-root-chord lengths away from the body surface. This permits imposing the undisturbed free-stream boundary conditions far enough from the body to permit accurate computation of subsonic flow. The far-field grid contains 51 axial, 39 circumferential, and 25 radial points.

A C-H grid topology was chosen for the F-18 wing, consisting of 139 chordwise, 41 spanwise, and 40 normal points. The wing grid was constructed in two steps. First, the 3DGRAPE elliptic grid generation code[28] was used to provide a grid with spacing normal to the wing surface appropriate for inviscid flow. Elliptic methods generally provide very smooth grids which can enhance the flow solver

convergence rate. Secondly, viscous grid clustering was obtained by redistributing grid points along coordinate lines normal to the body surface according to a stretching function described by Vinokur.[29] This function provides the grid clustering that minimizes the truncation error of a CFD algorithm for a fixed number of grid points. It was felt that this combination provided the best grid for achieving code robustness and solution accuracy.

The body-conforming fuselage grid is presented in Fig. 4; a ξ = constant plane from the fuselage grid in the vicinity of the wing is shown. As illustrated, those points of the fuselage grid that lie within the wing are cut out, forming a hole. The hole-boundary data of the fuselage grid are then supplied from the wing grid. Figure 5 shows the wing grid which overlaps the body grid in the region of the hole. Fringe points in the forebody grid obtain interpolated solution information from adjacent points in the wing grid. Similarly, the wing grid outer boundary points obtain information interpolated from the fuselage grid.

Boundary Conditions and Initial Conditions

For the isolated fuselage forebody computations, an adiabatic no-slip condition was applied at the body surface, while undisturbed free-stream conditions were maintained at the computational outer boundary. An implicit symmetry plane boundary condition was used at the circumferential edges of the fuselage grid, while at the downstream boundary a simple zero-axial-gradient extrapolation was applied. On the upstream spherical axis an extrapolation boundary condition was used to obtain the flow conditions on the axis from the cone of points one axial plane downstream.

The boundary conditions for the wing/fuselage geometry were largely the same as for the fuselage forebody geometry. However, in the Chimera code, an explicit symmetry plane boundary condition was used. In addition, a wing wake cut condition was applied by averaging the flow variables across the wake of the wing. This condition was applied both downstream of the wing trailing-edge and outboard of the wing-tip.

For both the fuselage and wing/fuselage computations, the flowfield was initially set to free-stream conditions throughout each grid. The flowfield was advanced sequentially in each component grid until a steady solution was obtained.

Chimera Solution Procedure

The Chimera approach has the advantage that a flow simulation code developed for a single grid (in this case the F3D code) can be adapted for composite overset grids. Control of the program is accomplished using the Pegasus code.[13]

At each time step, a grid and its data are fetched from an isolated memory into the working memory. Boundary interface arrays that store grid interconnect data, Q_{BC}, are also fetched. The Q_{BC} array holds overset-grid boundary values for the current grid, which are supplied from the adjacent grids. The solution on the current grid is updated using the flow algorithm and the applicable boundary conditions. The overset grid interface hole and outer boundary conditions are treated as explicit boundary conditions and are updated with trilinear interpolation. Overset boundary data that the current grid sends to other grids are then loaded into Q_{BC} and sent back to isolated memory. The process is then repeated for all the other grids to complete the time step.

Results and Discussion

Several numerical and physical factors can affect accurate prediction of high Reynolds number, high incidence flow. These include the effects of numerical smoothing, turbulence modeling, and the need for sufficiently fine grids to resolve the details of both the viscous boundary and the off-surface separated flow structure. A discussion of these factors for computations of flow over ogive-cylinder bodies is contained in Ref. 12. For the computations of flow over the F-18, the modified eddy-viscosity model[18] was used to model the effects of turbulence on the fuselage; the unmodified Baldwin-Lomax model[16] was used to model turbulence on the wing. The flow was assumed to be turbulent over the entire length of the aircraft, and no transition model was used. The radial grid spacing was chosen to give a value of $y^+ \approx 5$ at the first point above the body surface. This had been found necessary to properly resolve the viscous layer characteristics for a turbulent boundary layer.

Fuselage Forebody Predictions

In order to assess the ability of the F3D code to predict high-incidence flows about aircraft at full-scale flight conditions, and to assess the suitability of the computational grid topologies, several computations were carried out for turbulent flow about the F-18 fuselage forebody. These computations were obtained at flow conditions ($M_\infty = 0.34$, $\alpha = 19°$, $\mathrm{Re}_{\bar{c}} = 13.5 \times 10^6$ and $M_\infty = 0.2$, $\alpha = 30°$, $\mathrm{Re}_{\bar{c}} = 11.52 \times 10^6$) matching those of flight tests.[30-32] Computations for flow over the fuselage forebody of the F-18 at $\alpha = 30°$, obtained using the F3D code, have been reported previously.[1] However, comparison of these predictions with available flight test data, especially surface pressure measurements, is an on-going effort.

Predictions for $\alpha = 19°$

The numerical prediction of the surface flow pattern at $\alpha = 19°$ is shown in Fig. 6. These predictions are made using the two-block grid. The residuals were reduced a minimum of three orders of magnitude for both blocks. This required approximately 3500 time steps, and utilized approximately 10 hours of CRAY 2 CPU time. The flow over the LEX has a primary separation at the LEX leading-edge, forming a vortex over the upper surface of the LEX. The vortex creates a secondary crossflow separation line on the upper surface of the LEX, which is evident in Fig. 6. The surface streamlines show that there is little or no crossflow separation on the forebody of the fuselage, but a primary crossflow separation line is apparent under the LEX. This separation line is caused by the adverse circumferential pressure gradient field which the LEX exerts at high angles of attack.

The computed surface flow patterns may be compared with the surface flow visualization photo,[30] taken from flight tests conducted at the NASA Ames-Dryden Flight Research Facility,[31,32] presented in Fig. 7. This

visualization, analogous to wind-tunnel oil-flow visualization, was obtained by emitting a colored solvent (PGME) from orifices on the aircraft surface while the aircraft was stabilized at the desired test condition. The visualization shown was obtained for $\alpha = 19°$ and $Re_{\bar{c}} \approx 10.9 \times 10^6$. For this high Reynolds number case, the surface boundary layer transitions from laminar to turbulent flow upstream of the first circumferential ring of dye orifices. This is confirmed by the continuous, smooth behavior of the primary crossflow separation line seen in Fig. 7. Thus, assuming that the computed flow is turbulent over the entire body length is justified.

Note that the surface flow patterns from the numerical predictions are in good agreement with the flight test results. The flight test photograph (Fig. 7) shows that the flow is attached around the fuselage forebody (no obvious crossflow separation lines), with a primary crossflow separation line visible under the LEX, and a secondary separation line visible on the upper surface of the LEX. All of these features are to be found in the numerical prediction (Fig. 6), with the positions of the separation lines in very good agreement with those of the flight tests.

Figure 8 shows the numerical prediction of the LEX vortex as visualized with helicity density contours. Helicity density is defined as the scalar product of the local velocity and vorticity vectors.[33] Since it indicates both the strength and sense of rotation of the vortices, helicity density has been found to be an excellent means of visualizing the vortex pattern. By indicating positive and negative values of helicity density with different colors, it is easy to differentiate between the primary and secondary vortices. The off-surface flow pattern (Fig. 8) is consistent with the surface flow pattern shown in Fig. 6.

Comparisons of predicted surface pressures are compared with flight-test data[34] in Fig. 9 at five axial stations along the forebody; the data were taken from pressure taps located in circumferential rings at each axial station. The numerical predictions were made using a symmetry plane boundary condition, and were reflected for comparison with the flight-test data. Surface pressures are also presented at three axial stations on the LEX in Fig. 10. The flight test data were obtained at free-stream conditions of $M_\infty = 0.293$, $\alpha = 18.9°$, and $Re_{\bar{c}} = 12.0 \times 10^6$.

The predicted surface pressures on the forebody (Fig. 9) are seen to be in very good agreement with the flight-test data at all five axial stations ($x/\bar{c} = 0.069$, 0.177, 0.336, 0.590, and 0.893). The disagreement between the predicted and measured pressures at $x/\bar{c} = 0.590$ in the vicinity of $\phi \approx 100°$ and 260° is caused by the presence of antenna fairings on each side of the aircraft, located just forward of this axial station. These fairings were not modeled in the computational geometry. Similarly, the small differences at $x/\bar{c} = 0.893$ for $\phi \approx 180°$ are due to differences in the geometric modeling of the canopy, which is located just aft of this axial station. The canopy fairing is not modeled, and the canopy in the numerical grid begins slightly aft of the actual canopy location. These geometric differences cause the computed compression in the vicinity of the canopy at $x/\bar{c} = 0.893$ to be underpredicted.

The comparisons with the measured surface pressure data on the upper and lower surfaces of the LEX are presented in Fig. 10. Surface pressure data from both the starboard and port LEXs are presented, and show only minor differences due to asymmetries or sideslip. The predictions are seen to be in good agreement, especially at the most forward longitudinal station ($x/\bar{c} = 1.393$), with the accuracy of the prediction decreasing at the stations located further downstream ($x/\bar{c} = 1.704$ and 2.145). The predictions show the correct qualitative features at all the LEX stations. The grid resolution and the absence of the wing in the predictions could account for these differences, as will be discussed more fully for the $\alpha = 30°$ case.

Predictions for $\alpha = 30°$

Numerical predictions of flow about the F-18 fuselage forebody at $M_\infty = 0.2$, $\alpha = 30°$, and $Re_{\bar{c}} = 11.52 \times 10^6$, obtained using both the one-block and two-block grid topologies, were previously reported in Ref. 1. The computed surface flow patterns (Fig. 11) are seen to be in good agreement with the flight-test data (Fig. 12), especially for the position of the primary and secondary crossflow separation lines along the forebody, and the secondary crossflow separation line on the upper surface of the LEX. In addition, evidence of a crossflow separation line can be inferred from the PGME flow on the fuselage under the LEX. This separation is of particular importance, since the resulting vortex is in a position to be ingested by the engine inlets (see Fig. 12). The analogous comparison of computed[1] and measured[34] surface pressure distributions on the forebody and LEX are shown in Figs. 13 and 14, respectively.

Results computed using both grids show good agreement when compared with pressures at the five longitudinal stations on the forebody (Fig. 13). The one-block grid, which has a finer grid distribution in the leeward flow region than the two-block grid, shows very good prediction of the pressures in the vicinity of the primary and secondary separation lines, as well as on the leeward side of the secondary separation line. As with the $\alpha = 19°$ case, the disagreement between the pressures at $x/\bar{c} = 0.590$ at $\phi \approx 100°$ and 260° is caused by the presence of antenna fairings on each side of the aircraft. Similarly, the underprediction of the pressures at $x/\bar{c} = 0.893$ at $\phi \approx 180°$ is caused by small differences in canopy geometry.

The analogous comparison of predicted and measured pressures on the surface of the LEX (Fig. 14) is not as good as that on the forebody. Again, the one-block grid has a better overall comparison with the flight test data, mainly due to a finer grid distribution near the LEX leading edge. The one-block prediction shows good agreement with the pressures on the upper surface of the LEX between the leading edge and the secondary separation line. As shown for the $\alpha = 19°$ case, the predictions are in better agreement with the flight-test data at the most forward longitudinal stations on the LEX. The asymmetry in the flight-test data for $x/\bar{c} = 2.145$ may be due asymmetric vortex burst.

The computed pressure distributions underpredict the suction peak in the vicinity of the vortex on the leeward side of the LEX. One reason for this discrepancy may be a lack of circumferential grid resolution, particularly on the leeward surface of the LEX. Another possible source of error is the fact that the fuselage forebody computions do not include the presence of the wing, aft fuselage, or engine inlet. Including the upwash due to the wing in the vicinity of the LEX would cause the LEX to experience a higher angle of attack than the free-stream value of $\alpha = 30°$. The

upwash correction for this angle of attack, as measured in the flight tests, is approximately two degrees.[34] This increased angle of attack would induce a stronger LEX vortex, and thus lower pressures on the upper surface of the LEX. This would tend to make the computed values be in better agreement with the measured data. Also, flight-tests at this angle of attack show that the vortex has burst forward of $x/\bar{c} = 2.145$. The computation for the fuselage forebody does not predict a breakdown in the vortex, or the corresponding drop in the suction peak on the upper surface of the LEX.

Wing/Fuselage Prediction

A numerical prediction of the flow over the F-18 wing/fuselage at $M_\infty = 0.243$, $\alpha = 30.3°$, and $Re_{\bar{c}} = 10.0 \times 10^6$ was previously reported (Ref. 35) using the Chimera overset grid scheme described above. These flow conditions were chosen to match those of the flight tests.[32] The three grids (far-field, fuselage, and wing grids), containing a total of nearly 534,000 points, were initially solved in a non-time-accurate manner until the residuals leveled out after a reduction of one-and-a-half orders of magnitude. At this point it was apparent that further convergence of the flow solution over the wing/fuselage for this angle of attack would not be possible. The remainder of the calculations were performed in a time-accurate manner, with the residuals for the wing grid dropping a half order of magnitude very quickly after the time-accurate solution procedure was initiated. The residuals were reduced between two-and-a-half and three orders of magnitude, in total, after approximately 4300 time steps, utilizing approximately 50 hours of CRAY 2 CPU time. The numerical smoothing was reduced during the convergence to the smallest level possible that would yield a stable solution.

The predicted surface flow pattern and LEX vortex location for $\alpha = 30.3°$ are shown in Figs. 15 - 17. The predictions are compared with a flight test photograph taken at $\alpha = 30°$ (Fig. 18), where the surface flow is visualized on the wing and fuselage using tufts, and the LEX vortex is visualized with smoke injected into the flow near the LEX vertex. The predicted surface flow pattern (Figs. 15 and 16) show many interesting flow features. The secondary separation line on the upper surface of the LEX is seen to be in excellent agreement with the flow pattern in the flight test photograph, with another secondary separation line running along the side of the fuselage above the LEX. This separation line has been observed in the flight test, but is not readily visible in Fig. 18 due to the smoke obscuring the view, and the relative lack of tufts in this region.

The computed flow pattern on the upper surface of the wing (Fig. 15) shows the flow to be massively separated, with a strong spanwise component of outward flow, resulting from the LEX vortex, over the majority of the wing. A secondary separation line (the primary separation line is on the lower surface of the wing) has formed on the outboard half of the wing due to the presence of a fairly weak leading-edge vortex. There are also signs of a weak wing-tip vortex; a strong wing-tip vortex does not exist for in this case. These features are in qualitative agreement with the visualizations provided by the tufts in the flight-test photograph (Fig. 18). It should be noted that movies obtained during the flight tests indicate that at $\alpha = 30°$, the flow over the upper surface of the wing is highly unsteady. This unsteadiness is not as apparent when viewing the still photograph, but evidences of unsteadiness is visible in the random patterns of many of the tufts.

The computed lower surface flow pattern (Fig. 16) also shows several interesting features. A primary separation line is seen on the fuselage under the LEX. This separation line extends the entire length of the LEX and denotes the presence of a vortex flowing down the fuselage toward the engine inlet. The faired-over engine inlet geometry breaks up the vortex, but the primary separation line is re-established downstream of the engine inlet. A comment should be made about the predicted lower surface flow pattern. The primary crossflow separation line under the LEX runs downstream and a second primary separation line is seen to initiate. The first primary separation line then becomes a secondary crossflow separation line. This type of prediction is physically unrealistic, and has been found to be corrected with additional circumferential grid density.[12]

The flow on the lower surface of the wing shows a line of stagnation running the length of the leading edge, with fluid ahead of the line flowing around the leading-edge and over the upper surface of the wing. The flow downstream of the stagnation line proceeds smoothly over the remainder of the lower surface of the wing, with a slight outward spanwise flow apparent.

The computed LEX vortex location is shown in Fig. 17, and is compared with the flight-test location in Fig. 18. The most obvious feature of the flow is the breakdown of the LEX vortex in the vicinity of the wing/LEX junction. The adverse pressure gradient of the wing causes the computed LEX vortex to burst at $x/l = 0.49$. This vortex burst location occurs aft of the flight-test burst point ($x/l = 0.42$). However, it should be noted that the prediction is for an undeflected leading-edge flap on the wing, while the flight test had a leading-edge flap deflection. Also, the fineness of the fuselage grid has been shown to play a vital role in the accurate prediction of vortex burst location.[36] Coarser grids tend to delay the prediction of burst; a finer grid would tend to move the predicted vortex burst point forward.

Finally, comparisons of the computed LEX surface pressures, at $x/\bar{c} = 1.393$, are compared to the flight-test data[34] in Fig. 19. Also shown in Fig. 19 are the pressures computed for the isolated fuselage, from Fig. 14. The comparisons show that including the presence of the wing in the computation does in fact increase the suction peak on the leeward surface of the LEX, however, not to the levels shown by the flight test data. The differences may be due to a variety of factors. As mentioned previously, the current wing/fuselage predictions are made using a fairly coarse fuselage grid ($83 \times 63 \times 49$); a refined grid should enhance the accuracy of the prediction. Also, the wing/fuselage geometry utilized for the present computations does not accurately model the fuselage aft of the wing trailing-edge, and the empennage geometry is not included. Further, the current computational geometry has a faired-over engine inlet. Variation of engine throttle settings has been demonstrated in flight test[34] to have an effect on the vortex burst location. The logical next step for future study would be to improve the grid fineness, and to more accurately define the aircraft geometry.

Conclusions

The complex flow structures found in high-angle-of-attack flow about the F-18 HARV have been numerically predicted using a thin-layer Navier-Stokes code, F3D, in conjunction with the Chimera overset grid scheme. Predictions have been made for subsonic turbulent flow about the F-18 fuselage forebody and the combined wing/fuselage. The computed results have been shown to be in good agreement with flight-test flow visualization and surface-pressure measurements, and give detailed information about the behavior of three-dimensional separated and vortical flows about realistic aircraft geometries.

The computations have shown that the prediction of high-angle-of-attack flow over realistic aircraft geometries is at hand. The ability of the thin-layer Navier-Stokes code to accurately predict the flow field features such as the forebody and LEX primary and secondary vortices, as well as the onset of LEX vortex breakdown, has been demonstrated. Future improvements in the details of the aircraft geometry, such as adding the empennage, inlet, and wing leading-edge flap, as well as increased grid resolution, should result in a realistic and detailed numerical description of the flow over the HARV at high angles of attack.

Acknowledgements

The authors would like to thank Dave Fisher and John Del Frate of the Ames-Dryden Flight Research Facility for supplying a variety of published and unpublished flight test and wind tunnel data.

References

[1] Schiff, L. B., Cummings, R. M., Sorenson, R. L., and Y. M. Rizk, "Numerical Simulation of High-Incidence Flow over the F-18 Fuselage Forebody," AIAA Paper 89-0339, AIAA 27th Aerospace Sciences Meeting, Jan. 1989.

[2] Thomas, J. L., Walter, R. W., Reu, T., Ghaffari, F., Weston, R. P., and Luckring, J. M., "A Patched-Grid Algorithm for Complex Configurations Directed Towards the F-18 Aircraft," AIAA Paper 89-0121, AIAA 27th Aerospace Sciences Meeting, Jan. 1989.

[3] Ghaffari, F., Luckring, J. M., and Thomas, J. L., "Navier-Stokes Solutions About the F-18 Forebody-Strake Configuration," AIAA Paper 89-0338, AIAA 27th Aerospace Sciences Meeting, Jan. 1989.

[4] Fujii, K. and Obayashi, S., "Computations of Three-Dimensional Viscous Transonic Flows Using the LU–ADI Factored Scheme," Technical Report of the Japanese National Aerospace Laboratory, TR–889T, 1985.

[5] Newsome, R. W. and Adams, M. S., "Numerical Simulation of Vortical-Flow over an Elliptical-Body Missile at High Angles of Attack," AIAA Paper 86–0559, AIAA 24th Aerospace Sciences Meeting, Jan. 1986.

[6] Pan, D. and Pulliam, T. H., "The Computation of Steady Three-Dimensional Separated Flows over Aerodynamic Bodies at Incidence and Yaw," AIAA Paper 86–0109, AIAA 24th Aerospace Sciences Meeting, Jan. 1986.

[7] Kordulla, W., Vollmers, H., and Dallmann, U., "Simulation of Three-Dimensional Transonic Flow with Separation Past a Hemisphere-Cylinder Configuration," AGARD CPP–412, *Applications of Computational Fluid Dynamics in Aeronautics*, Paper 31, April 1986.

[8] Ying, S. X., Schiff, L. B., and Steger, J. L., "A Numerical Study of Three-Dimensional Separated Flow Past a Hemisphere-Cylinder," AIAA Paper 87–1207, AIAA 19th Fluid Dynamics, Plasma Dynamics, and Lasers Conference, June 1987.

[9] Fujii, K. and Schiff, L. B., "Numerical Simulation of Vortical Flows Over a Strake-Delta Wing," AIAA Paper 87–1229, AIAA 19th Fluid Dynamics, Plasma Dynamics, and Lasers Conference, June 1987.

[10] Vatsa, V. N., Thomas, J. L., and Wedan, B. W., "Navier- Stokes Computations of Prolate Spheroids at Angle of Attack," AIAA Paper 87–2627, AIAA 14th Atmospheric Flight Mechanics Conference, August 1987.

[11] Steger, J. L., Ying, S. X., and Schiff, L. B., "A Partially Flux-Split Algorithm for Numerical Simulation of Unsteady Viscous Flows," Proceedings of a Workshop on Computational Fluid Dynamics, University of California, Davis, 1986.

[12] Schiff, L. B., Degani, D. and Cummings, R. M., "Numerical Simulation of Separated and Vortical Flows on Bodies at Large Angles of Attack," Fourth Symposium on Numerical and Physical Aspects of Aerodynamic Flows, Jan. 1989.

[13] Benek, J. A., Buning, P. G., and Steger, J. L., "A 3-D Chimera Grid Embedding Technique," AIAA Paper 85-1523, AIAA 7th Computational Fluid Dynamics Conference, July 1985.

[14] Steger, J. L. and Benek, J. A., "On the use of Composite Grid Schemes in Computational Aerodynamics," *Comp. Methods in Applied Mech. and Engr.*, Vol. 64, October 1987, pp. 301-320.

[15] Viviand, H., "Conservative Forms of Gas Dynamics Equations," *La Recherche Aerospatiale* **1** (1974), 65–68.

[16] Baldwin, B. S. and Lomax, H., "Thin Layer Approximation and Algebraic Model for Separated Turbulent Flows," AIAA Paper 78-257, AIAA 16th Aerospace Sciences Meeting, Jan. 1978.

[17] Steger, J. L., "Implicit Finite-Difference Simulation of Flow About Arbitrary Two-Dimensional Geometries," *AIAA Journal* **16** (1978), 679–686.

[18] Degani, D. and Schiff, L. B., "Computation of Turbulent Supersonic Flows Around Pointed Bodies Having Crossflow Separation," *J. Comp. Phys.* **66** (1986), 173–196.

[19] Cebeci, T., Smith, A. M. O., and Mosinkis, G., "Calculation of Compressible Adiabatic Turbulent Boundary Layers," *AIAA Journal* **8** (1970), 1974–1982.

[20] Steger, J. L. and Warming, R. F., "Flux Vector Splitting of the Inviscid Gasdynamic Equations with Applications to Finite-Difference Methods," *J. Comp. Phys.* **40** (1981), 263–293.

[21] Ying, S. X., "Three-Dimensional Implicit Approximately Factored Schemes for Equations in Gasdynamics," Ph.D. Thesis, Stanford University, 1986 (also SUDAAR 557, June 1986).

[22] Buning, P. G., Chiu, I. T., Obayashi, S., Rizk, Y. M., and Steger, J. L., "Numerical Simulation of the Integrated Space Shuttle Vehicle in Ascent," AIAA Paper 88-4359, AIAA Atmospheric Flight Mechanics Conference, Aug. 1988.

[23] Kaynak, U., Holst, T. L., and Cantwell, B. J., "Computation of Transonic Separated Wing Flows Using an Euler/Navier-Stokes Zonal Approach," NASA TM 88311, July 1986.

[24] Flores, J. and Chaderjian, N. M., "The Numerical Simulation of Transonic Separated Flow about the Complete F-16A," AIAA Paper 88-2506, AIAA 6th Applied Aerodynamics Conference, June 1988.

[25] Reznick, S., "Transonic Navier-Stokes Computations of Strake-Generated Vortex Interactions for a Fighter-Like Configuration," NASA TM 100009, Feb. 1988.

[26] Luh, R. C. C., "Surface Grid Generation for Complex Three-Dimensional Geometries," NASA TM 101046, Oct. 1988.

[27] Steger, J. L and Rizk, Y. M., "Generation of Three Dimensional Body Fitted Coordinates Using Hyperbolic Partial Differential Equations," NASA TM 86753, June 1985.

[28] Sorenson, R. L., "Three-Dimensional Zonal Grids About Arbitrary Shapes by Poisson's Equation," in *Numerical Grid Generation in Computational Fluid Mechanics '88*, Pineridge Press Ltd., Swansea, U. K., 1988 (Also, NASA TM 101018, August 1988).

[29] Vinokur, M., "On One-Dimensional Stretching Functions for Finite Difference Calculations," NASA CR 3313, 1980.

[30] Fisher, D. F., Richwine, D. M., and Banks, D. W., "Surface Flow Visualization of Separated Flows on the Forebody of an F-18 Aircraft and Wind-Tunnel Model," NASA TM 100436, May 1988.

[31] Fisher, D. F. and Meyer, R. R., Jr., "Flow Visualization Techniques for Flight Research," NASA TM 100455, Oct. 1988.

[32] Fisher, D. F., Del Frate, J. H., and Richwine, D. M., "In-Flight Visualization Characteristics of the NASA F-18 High Alpha Research Vehicle at High Angles of Attack," SAE Paper 892222, SAE Aerospace Technology Conference and Exposition, Sep. 1989.

[33] Levy, Y., Seginer, A., and Degani, D., "Graphical Representation of Three-Dimensional Vortical Flows by Means of Helicity Density and Normalized Helicity," AIAA Paper 88–2598, AIAA 6th Applied Aerodynamics Conference, June 1988.

[34] Fisher, D. F., private communication, 1989.

[35] Cummings, R. M., Rizk, Y. M., Schiff, L. B., and Chaderjian, N. M., "Navier-Stokes Predictions of the Flowfield Around the F-18 (HARV) Wing and Fuselage at Large Incidence," AIAA Paper 90-0099, AIAA 28th Aerospace Sciences Meeting, Jan. 1990.

[36] Ekaterinaris, J. A. and Schiff, L. B., "Vortical Flows over Delta Wings and Numerical Prediction of Vortex Breakdown," AIAA Paper 90-0102, AIAA 28th Aerospace Sciences Meeting, Jan. 1990.

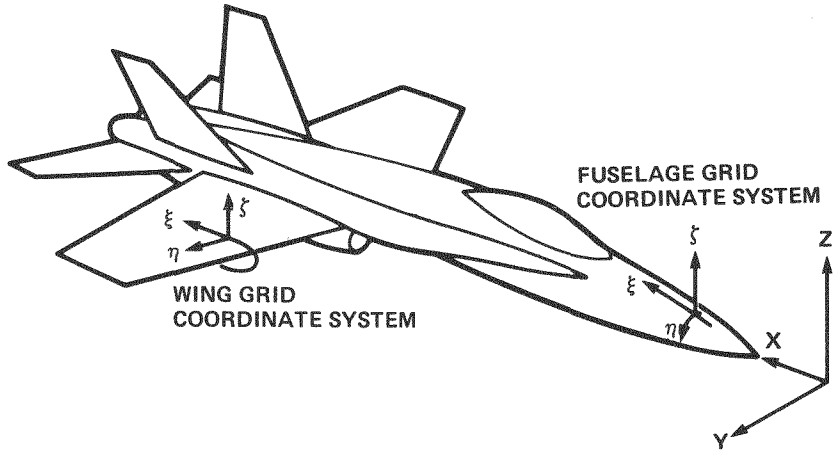

Fig. 1. Coordinates and notation.

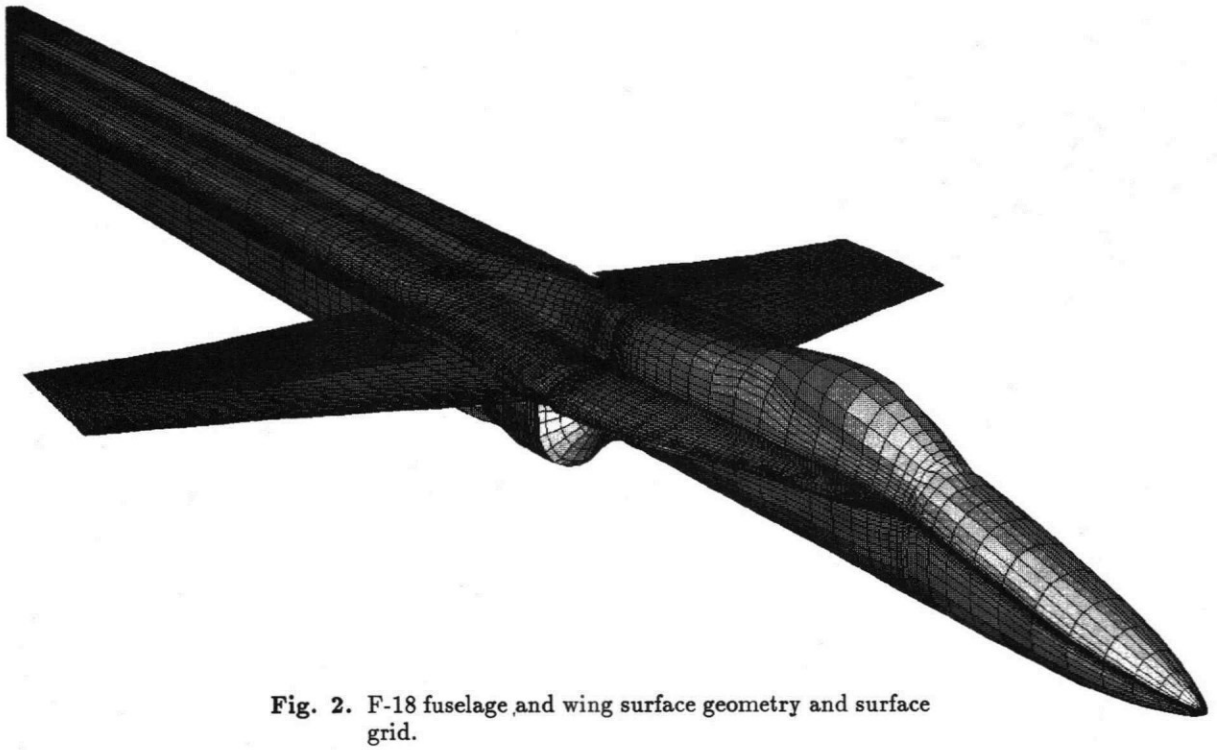

Fig. 2. F-18 fuselage and wing surface geometry and surface grid.

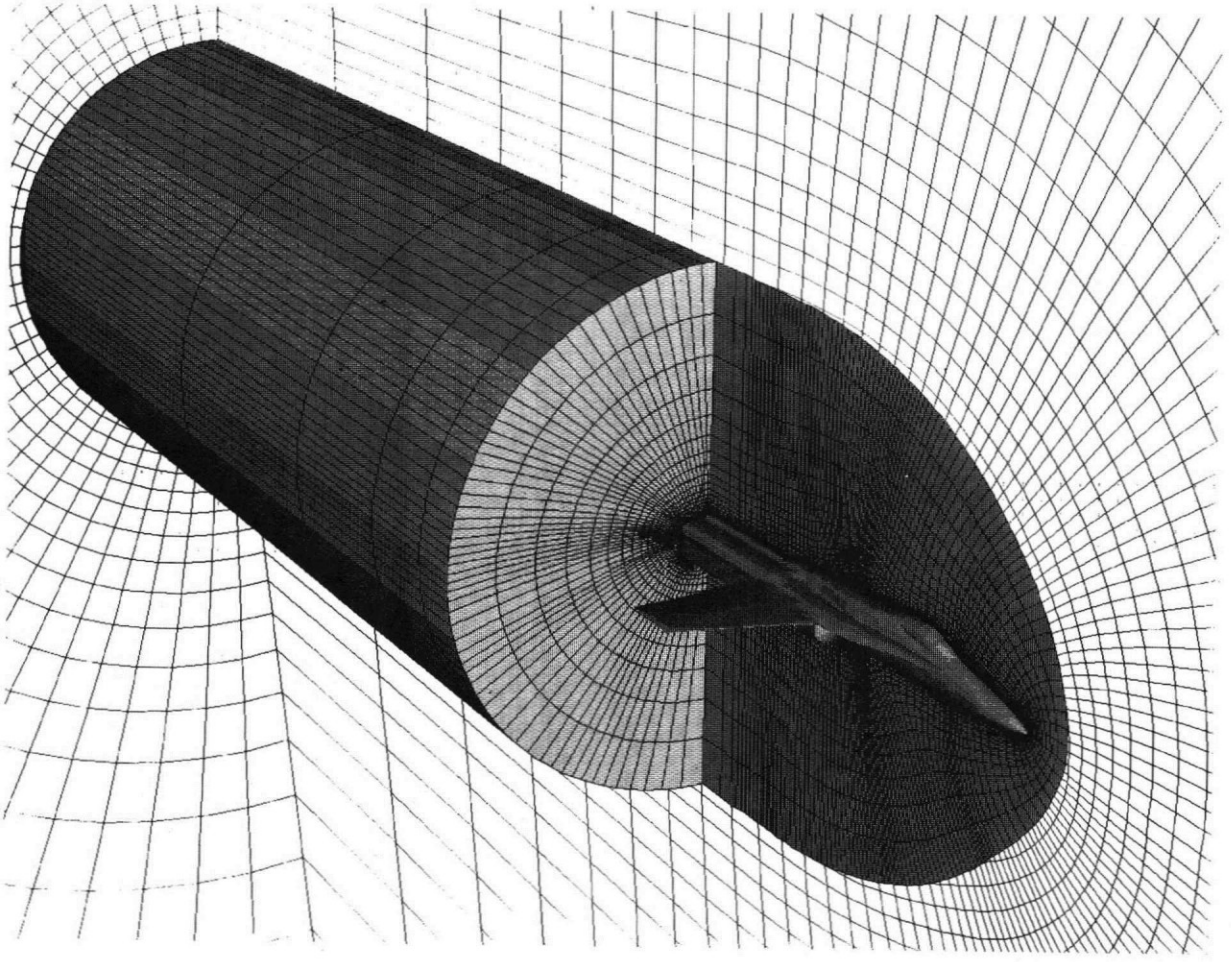

Fig. 3. Wing/fuselage Chimera grid system.

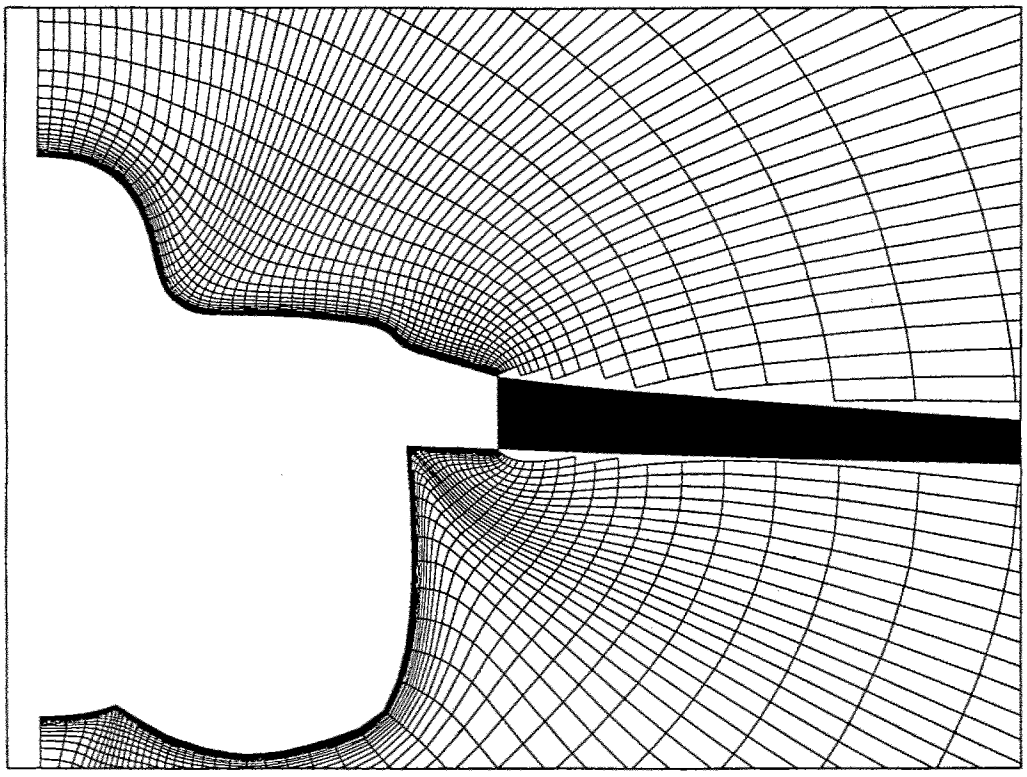

Fig. 4. Fuselage grid hole in the vicinity of the wing surface.

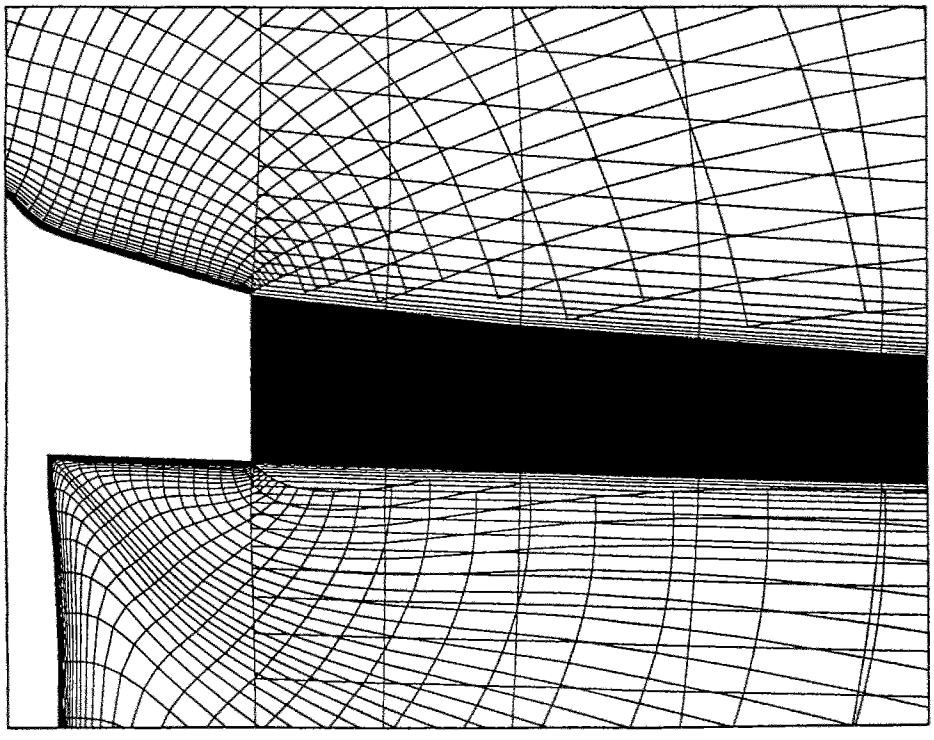

Fig. 5. Wing and fuselage grid overlap.

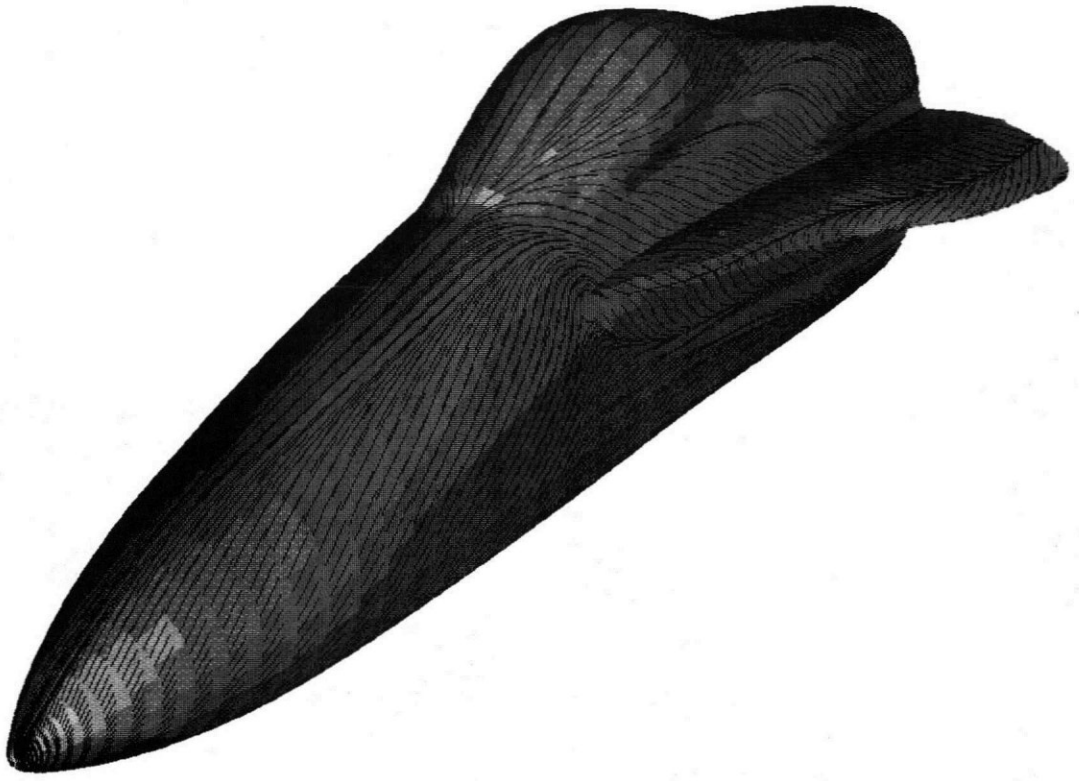

Fig. 6. Fuselage forebody predicted surface flow pattern; $M_\infty = 0.2$, $\alpha = 19°$, $Re_\ell = 11.52 \times 10^6$.

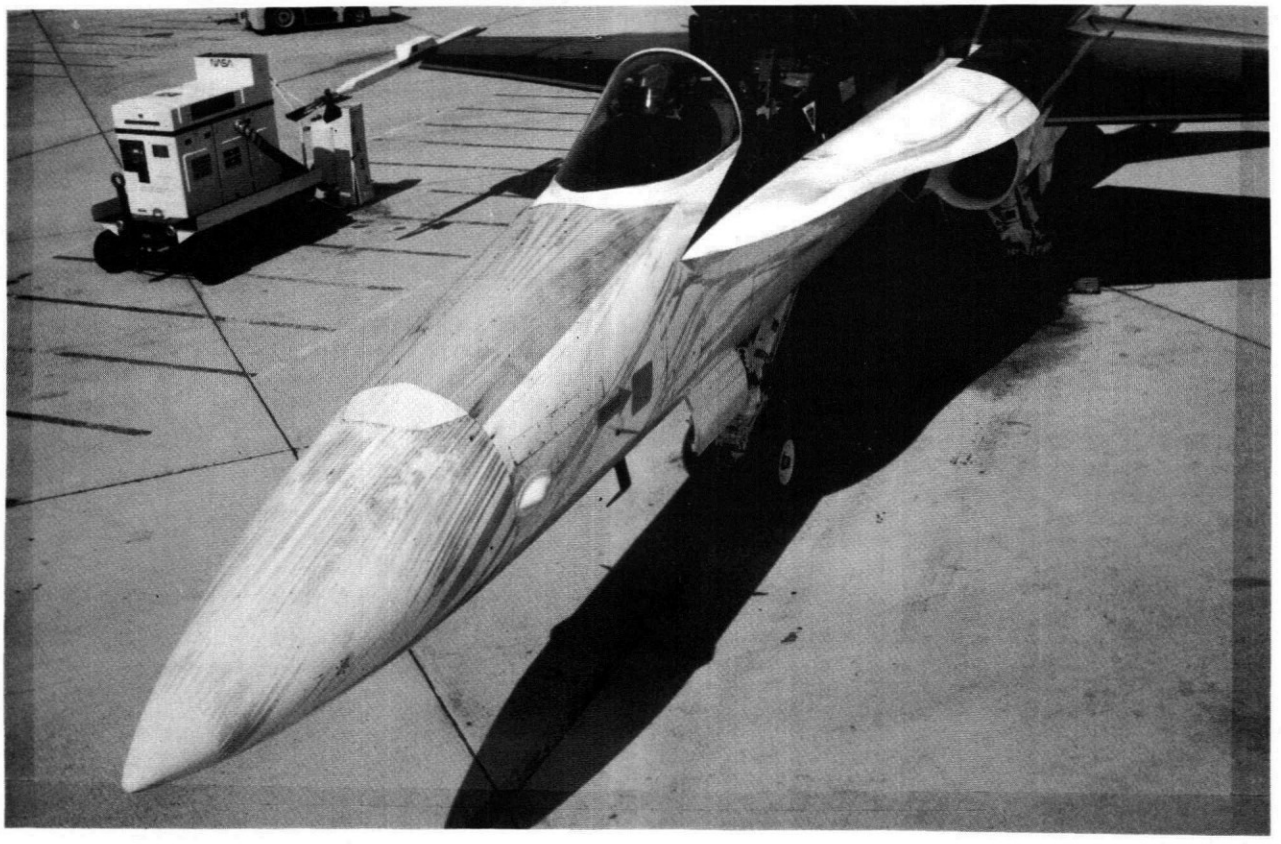

Fig. 7. Flight test surface flow pattern; $\alpha = 19°$ (Ref. 30).

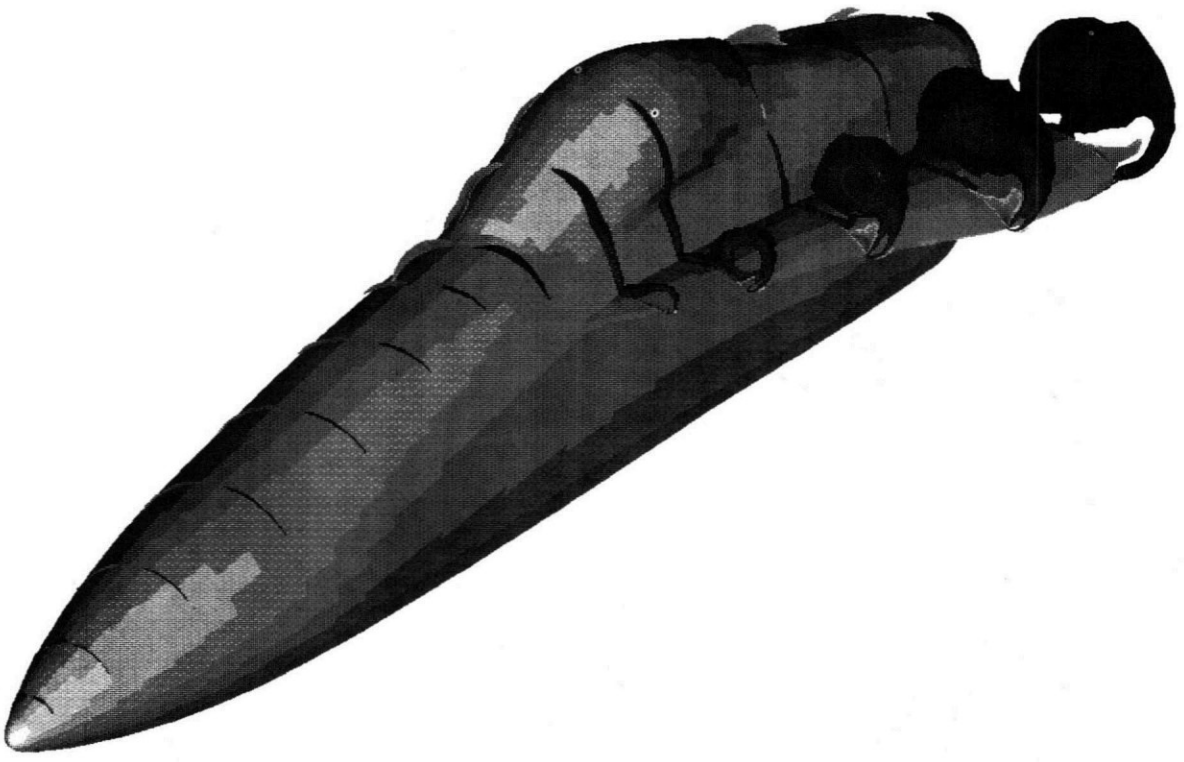

Fig. 8. Fuselage forebody predicted helicity density contours; $M_\infty = 0.2$, $\alpha = 19°$, $Re_{\bar{c}} = 11.52 \times 10^6$.

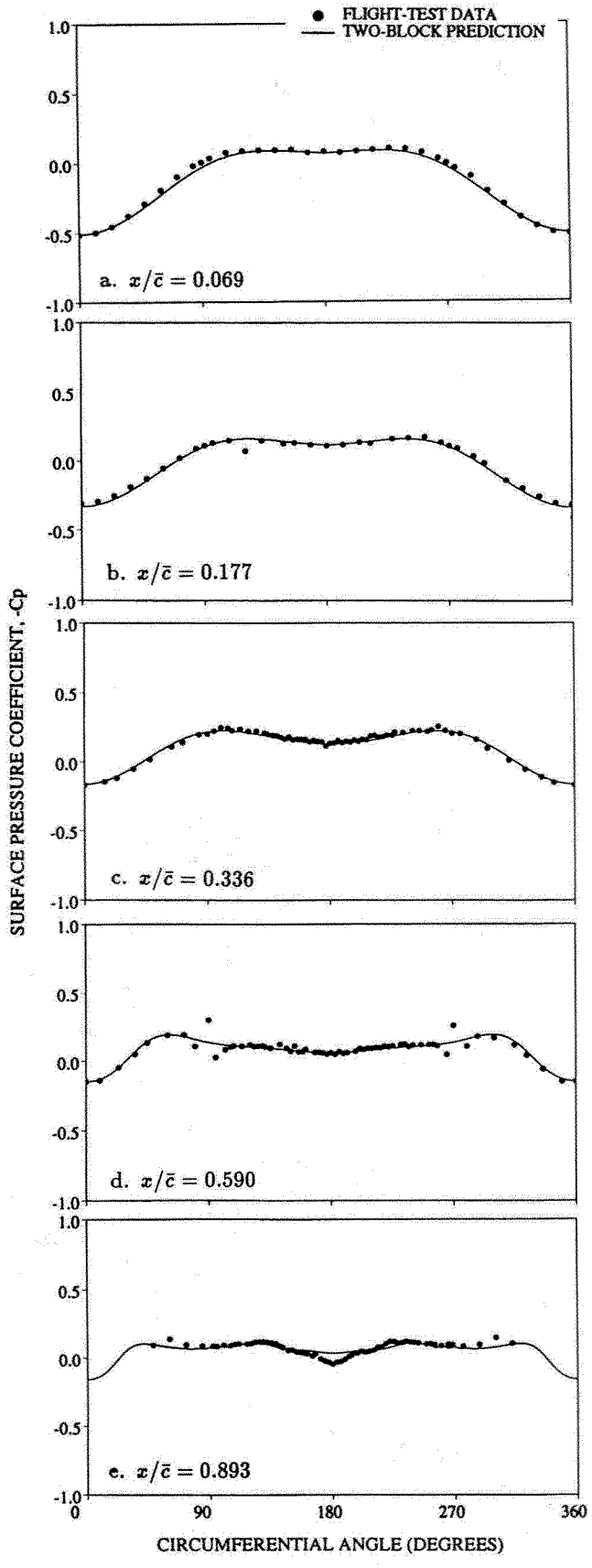

Fig. 9. Fuselage forebody surface pressure predictions compared with flight test data on forebody; $\alpha = 19°$.

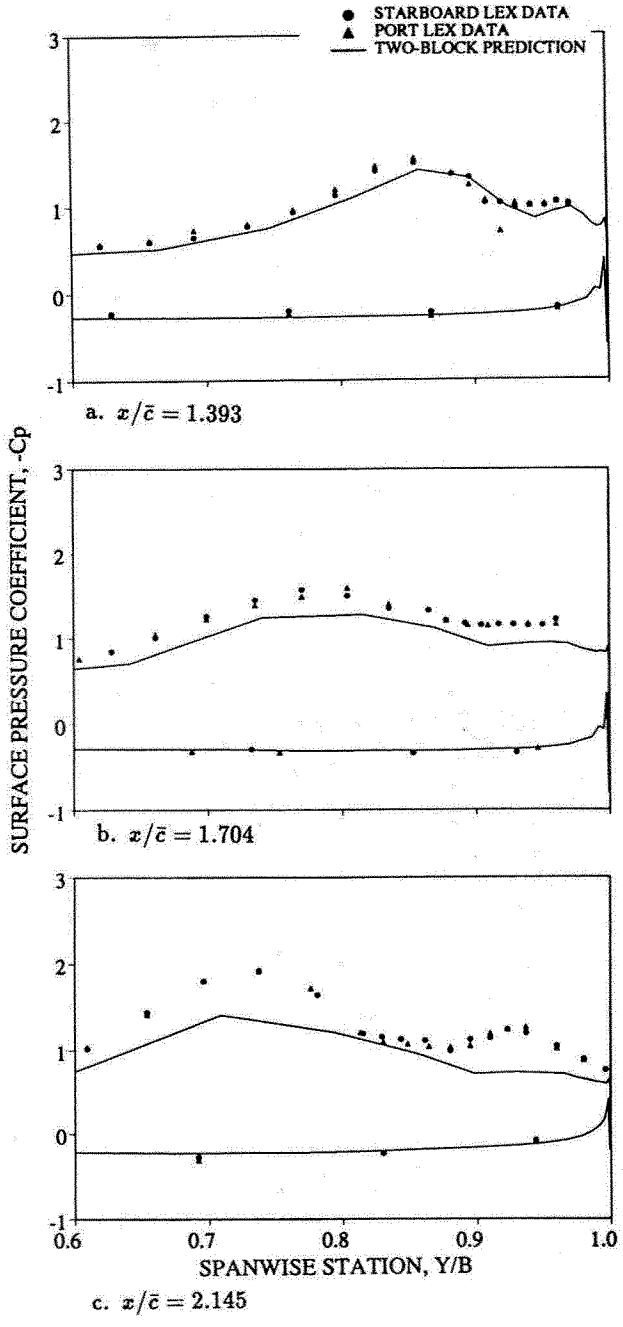

Fig. 10. Fuselage forebody surface pressure predictions compared with flight test data on LEX; $\alpha = 19°$.

Fig. 11. Fuselage forebody predicted surface flow pattern; $M_\infty = 0.2$, $\alpha = 30°$, $Re_{\bar{c}} = 11.52 \times 10^6$.

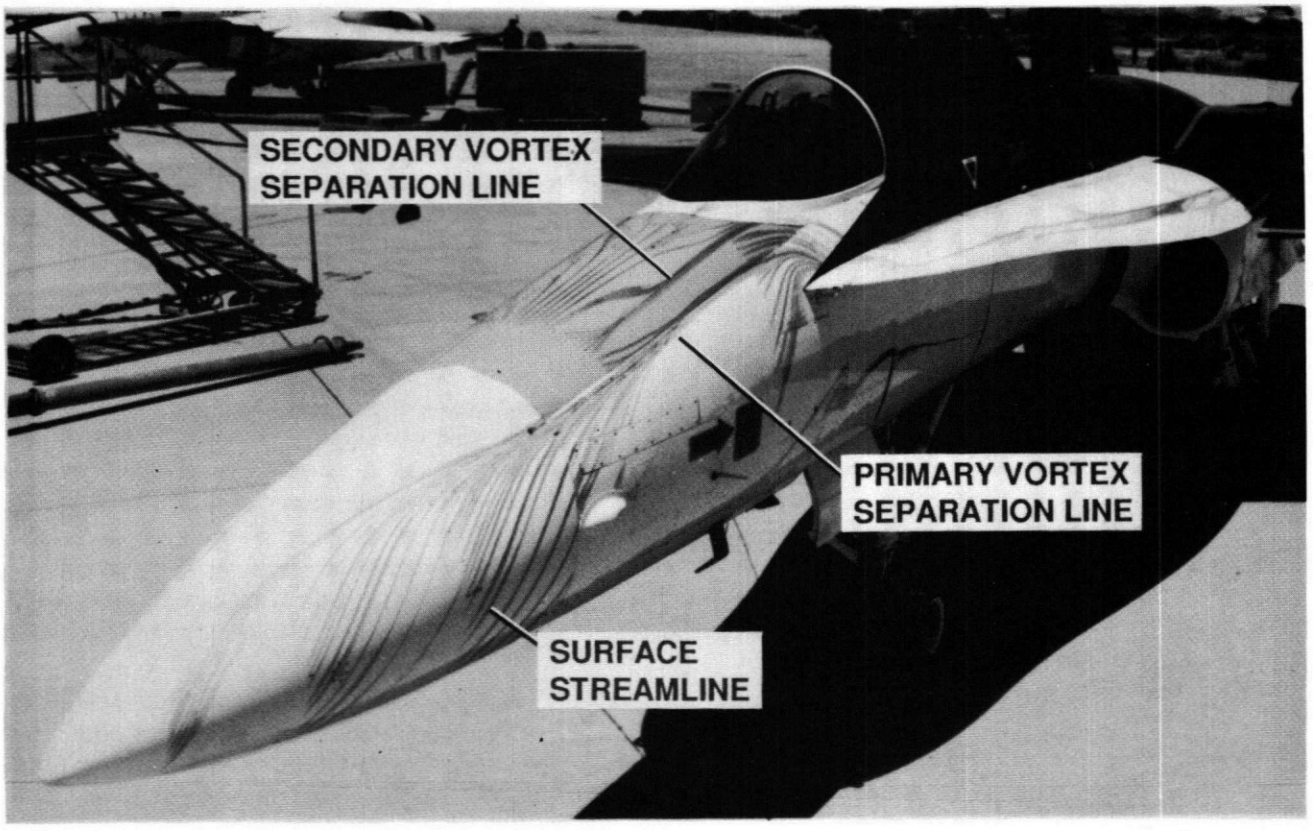

Fig. 12 Flight test surface flow pattern; $\alpha = 30°$ (Ref. 30).

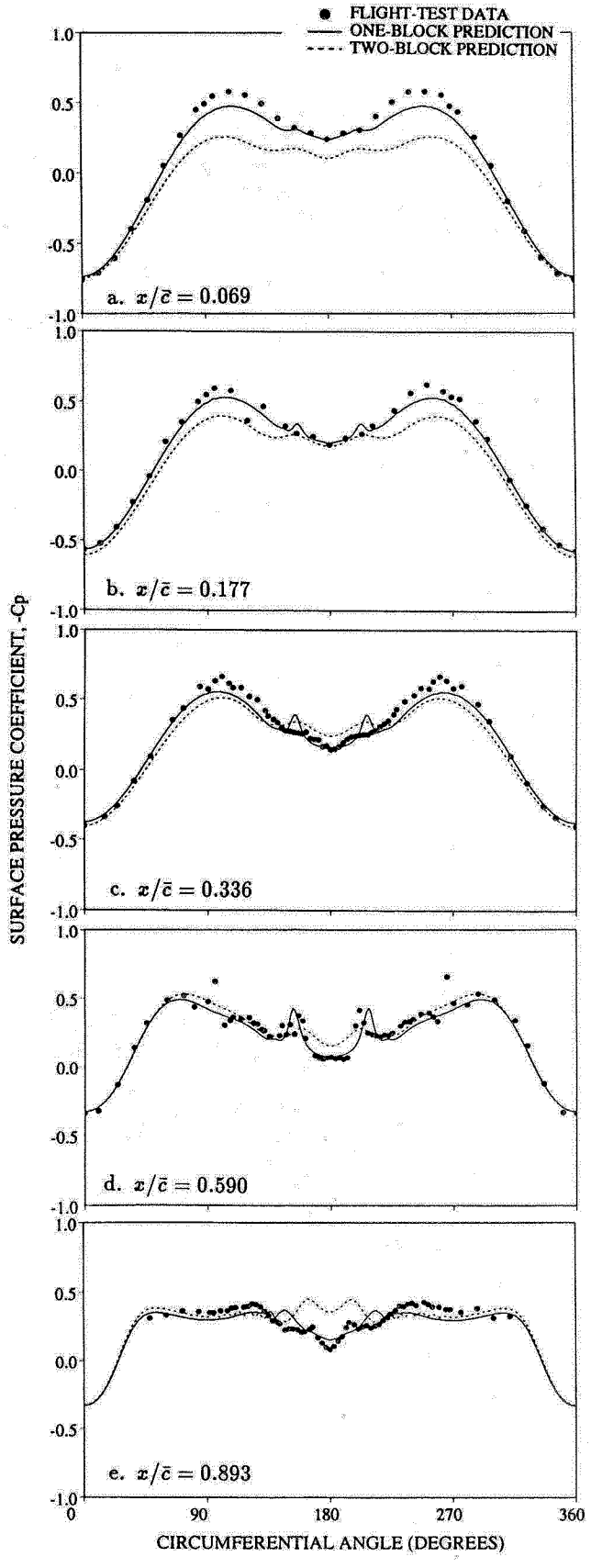

Fig. 13. Fuselage forebody surface pressure predictions compared with flight test data on forebody; $\alpha = 30°$.

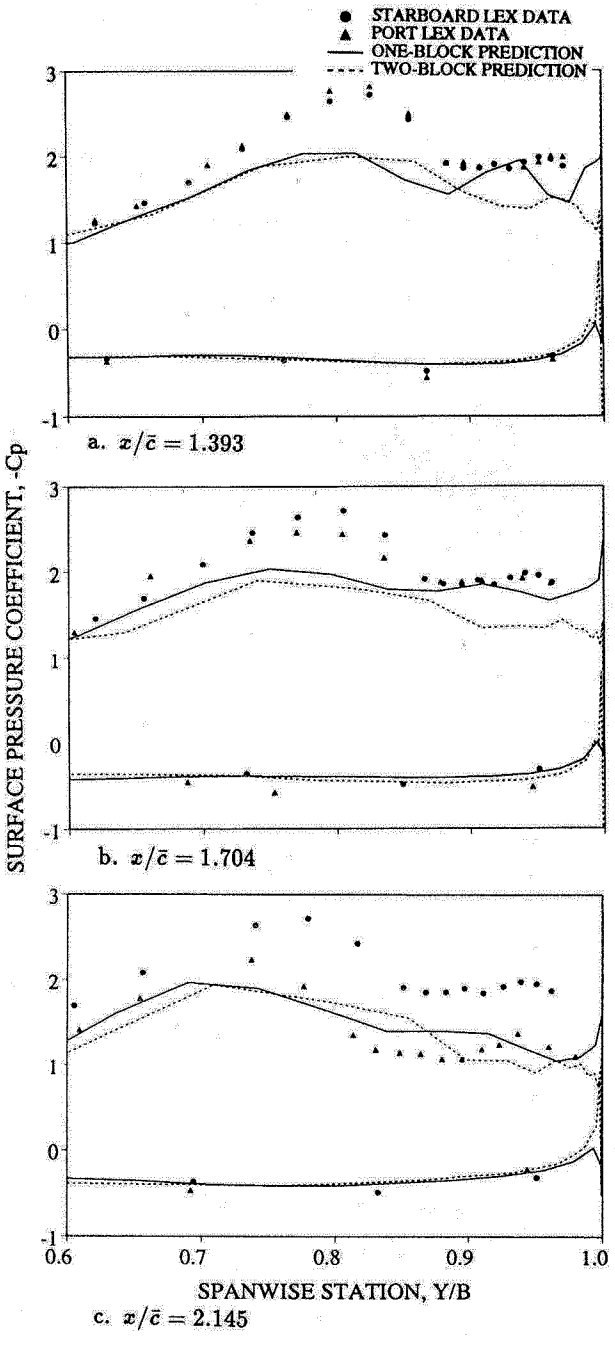

Fig. 14. Fuselage forebody surface pressure predictions compared with flight test data on LEX; $\alpha = 30°$.

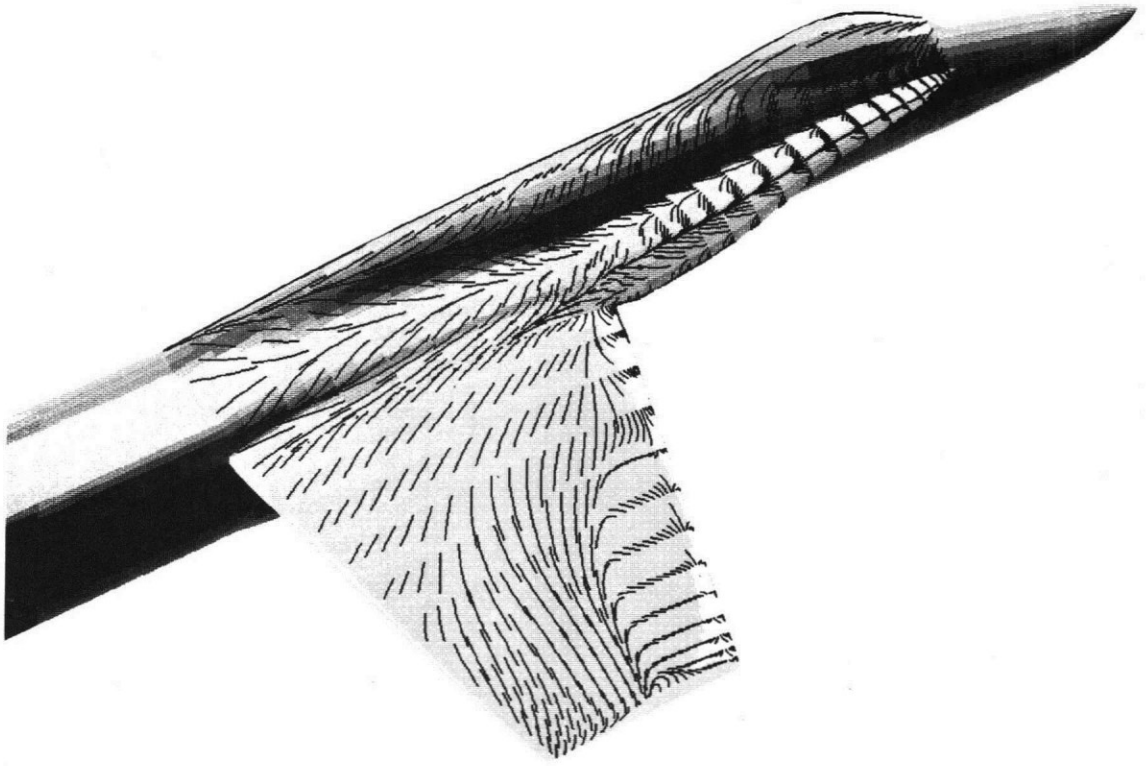

Fig. 15. Wing/fuselage predicted upper surface flow pattern; $M_\infty = 0.243$, $\alpha = 30.3°$, $Re_{\bar{c}} = 10.0 \times 10^6$.

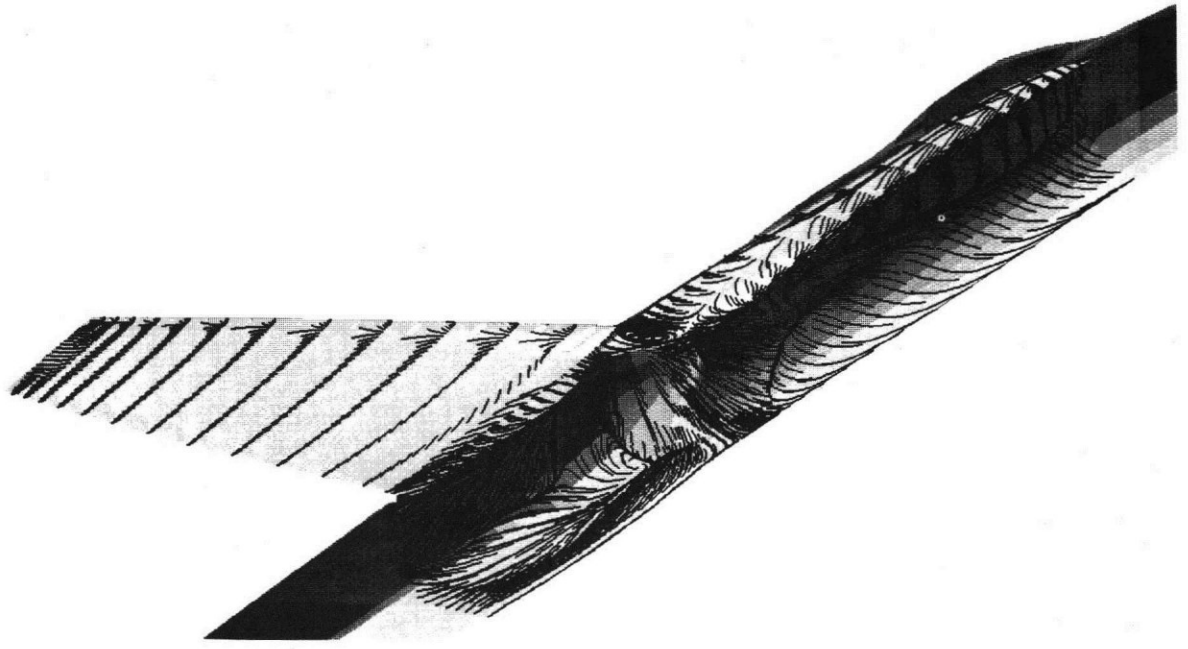

Fig. 16. Wing/fuselage predicted lower surface flow pattern; $M_\infty = 0.243$, $\alpha = 30.3°$, $Re_{\bar{c}} = 10.0 \times 10^6$.

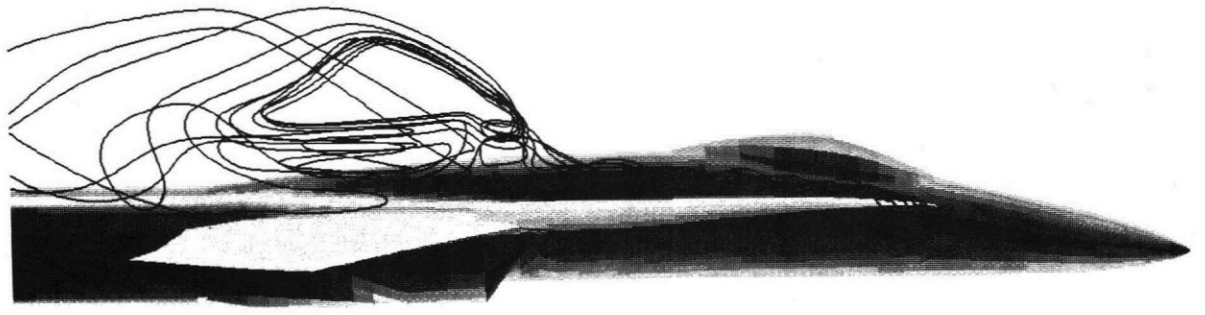

Fig. 17. Wing/fuselage predicted LEX vortex; $M_\infty = 0.243$, $\alpha = 30.3°$, $Re_{\bar{c}} = 10.0 \times 10^6$.

Fig. 18. Flight test surface flow pattern and smoke-flow vortex visualization; $\alpha = 30°$ (Ref. 31).

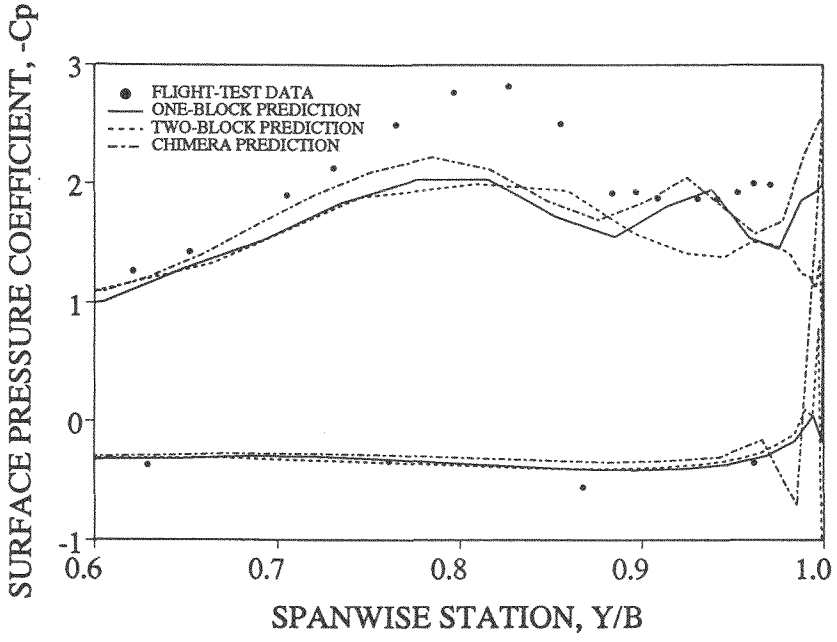

Fig. 19. Wing/fuselage surface pressure predictions compared with flight test data on LEX; $\alpha = 30.3°$.